Structural Characteristics of Lithium Nickel Phosphate Studied Using Analytical Electron Microscopy and Raman Spectroscopy

C. V. Ramana,*,[†] A. Ait-Salah,[‡] S. Utsunomiya,[†] U. Becker,[†] A. Mauger,[‡] F. Gendron,[‡] and C. M. Julien[‡]

Nanoscience and Surface Chemistry Laboratory, Department of Geological Sciences, University of Michigan, Ann Arbor, Michigan 48109, and Institut des Nano-Sciences de Paris (INSP), Université Pierre et Marie Curie, CNRS-UMR 7588, campus Boucicaut, 140 rue de Lourmel, 75015 Paris, France

The structural characteristics of lithium nickel phosphate ($LiNiPO_4$) prepared by solid-state chemical reaction have been studied in detail using the analytical electron microscopy and Raman spectroscopy measurements. The high-resolution transmission electron microscopy and selected area electron diffraction measurements indicate that the grown $LiNiPO_4$ is well-crystallized in olivine structure without any indication of crystallographic defects such as dislocations or misfits. The energy-dispersive X-ray spectrometry coupled with the elemental compositional mapping using high-angle angular dark field scanning electron microscopy confirms the chemical quality of the grown $LiNiPO_4$ in terms of homogeneity and uniform elemental distribution characteristics. The local structure and chemical bonding between NiO_6 octahedral and $(PO_4)^{3-}$ tetrahedral groups probed by Raman spectroscopy also indicate the high-quality of $LiNiPO_4$. Structural analysis of the delithiated $Li_{0.09}NiPO_4$ phase indicates lattice contraction and distortion upon lithium extraction. A detailed analysis and comparison of the pristine and delithiated phases is also reported.

I. Introduction

The large family of compounds of the $ABPO_4$ type (with A and B being mono- and divalent cations, respectively) exhibits different frameworks depending on the relative size of the A and B ions, for example, arcanite-, trydimite-, or olivine-type structures. For the A ions of small size, as in the case of Li^+, the resulting compounds, lithium transition-metal phosphates ($LiMPO_4$ with M = Fe, Ni, Co, Mn) adopt the olivine-like (Mg_2SiO_4) structure containing high-spin M^{2+} ions.[1] These phosphates exhibit a variety of structural features,[2−4] the most prominent of which is the existence of tunnels in which small ions can move freely, a property that makes them potential hosts for the insertion and extraction of ions. As a result of their high capacity, good thermal stability, and environmental benignity, these compounds have been proposed as alternative electrode materials for rechargeable lithium-ion batteries.[1,5−10]

The crystal structure of $LiNiPO_4$ is made up of two types of polyhedra, distorted NiO_6 octahedral units that are corner shared and cross-linked with the PO_4 tetrahedral oxo-anions, forming a three-dimensional network with tunnels that are occupied by Li ions along the (010) and (001) directions. In this network, nearly close-packed oxygen atoms in hexagons can be found with Li and Ni ions that are located at the center of octahedral sites.[2] A schematic representation of the olivine structure is shown in Figure 1. As a result of this typical structural configuration, it is believed that the strong covalent PO_4 unit tends to reduce the covalency of the M−O bond, modifying the redox potential for the $M^{2+/3+}$ couple and thus producing a useful potential for lithium extraction and reinsertion.[11]

Recently, there has been a great deal of interest in lithium nickel phosphates. Different aspects, such as synthesis, structural and vibrational properties, electrochemistry, and magnetism, of these materials have been studied by various research groups using both experimental and theoretical invetigations.[12−35] The advancement in lithium battery technology is envisaged on the basis of lithium metal phosphate

* Corresponding author. E-mail: ramanacv@umich.edu. Tel.: 734-763-5344. Fax: 734-763-4690.
† University of Michigan.
‡ Université Pierre et Marie Curie.

(1) Padhi, A. K.; Nanjundaswamy, K. S.; Goodenough, J. B. *J. Electrochem. Soc.* **1997,** *144,* 1188.
(2) Séller, S.; Duran, J. L. *Acta Crystallogr.* **1960,** *18,* 258.
(3) Santoro, R. P.; Segal, D. J.; Newnham, R. E. *J. Phys. Chem. Solids* **1966,** *27,* 1192.
(4) Vankin, D.; Zaretsky, J. L.; Ostenson, J. E.; Chakoumakos, B. C.; Goni, A.; Pagliuso, P. J.; Rojo, T.; Barberis, G. E.; *Phys. Rev. B* **1999,** *60,* 1100.
(5) Yamada, A.; Chung, S. C.; Hinokuma, K. *J. Electrochem. Soc.* **2001,** *148,* A224.
(6) Zaghib, K.; Striebel, K.; Guerfi, A.; Shim, J.; Armand, M.; Gauthier, M. *Electrochim. Acta* **2004,** *50,* 263.
(7) Dai, D.; Whangbo, M.-H.; Koo, H.-J.; Rocquefelte, X.; Jobic, S.; Villesuzanne, A. *Inorg. Chem.* **2005,** *44,* 2407.
(8) Islam, M. S.; Driscoll, D. J.; Fisher, C. A. J.; Slater, P. R. *Chem. Mater.* **2005,** *17,* 5085.
(9) Tucker, M. C.; Doeff, M. M.; Richardson, T. J.; Finones, R.; Cairns, E. J.; Reimer, J. A. *J. Am. Chem. Soc.* **2002,** *124,* 3832.
(10) Masquelier, C.; Padhi, A. K.; Nanjundaswamy, K. S.; Goodenough, J. B. *J. Solid State Chem.* **1998,** *135,* 228.
(11) Tucker, M. C.; Doeff, M. M.; Richardson, T. J.; Finones, R.; Reimer, J. A.; Cairns, E. J. *Electrochem. Solid-State Lett.* **2002,** *5,* A95.
(12) Ritchie, A. G. *J. Power Sources* **2004,** *142,* 285.
(13) Wolfenstine, J.; Allen, J. *J. Power Sources* **2005,** *142,* 389.
(14) Wolfenstine, J.; Allen, J. *J. Power Sources* **2004,** *136,* 150.
(15) Herle, P. S.; Ellis, B.; Coombs, N.; Nazar, L. F. *Nat. Mater.* **2004,** *3,* 147.
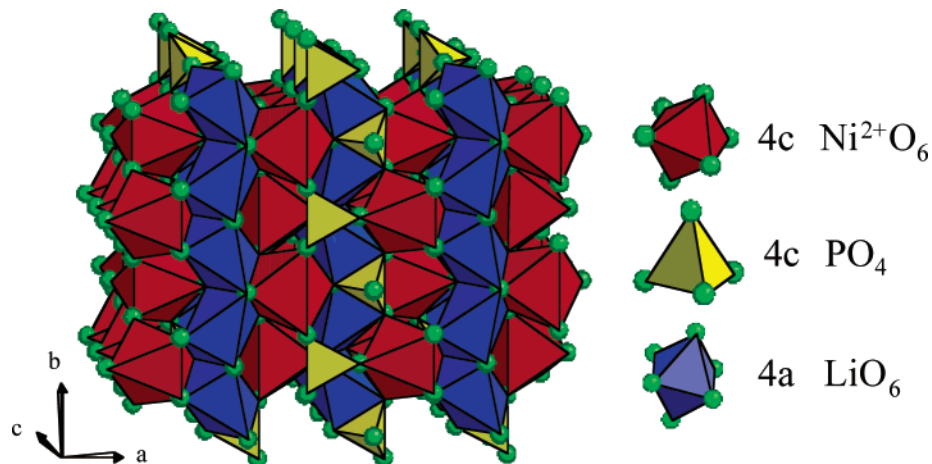
Figure 1. Schematic representation of the olivine-like structure showing the three-dimensional network formed by cross-linked NiO_6 and PO_4 polyhedra.

materials as cathode materials.[6,8,12–16] The first principle calculations, using various approaches, have confirmed the high electrochemical potentials of LiNiPO₄, which makes them attractive for application in lithium battery technology.[17–20] The extensive contributions of Ceder's research group using first principles computations, which are based on local density approximation (LDA) and generalized gradient approximation (GGA), have predicted the Li intercalation potential of LiNiPO₄ to be above 5 V.[19,20] Wolfenstine and Allen have recently performed experiments and verified the higher potentials predicted by theoretical predications.[13] On the other hand, alternate methods such as formation of a nano-network of metal phosphides, metal phosphocarbides, and/or amorphous carbon at grain boundaries have been proposed to increase the electrical conductivity of these materials.[15] However, most of the recent experimental and theoretical studies have been focused on the magnetic properties and/or single-crystal LiNiPO₄ materials.[4,7,21–31]

The emphasis in this work is the synthesis and structural characterization of LiNiPO₄ as in the design of new electrode materials an understanding of the structural features and the morphology is of crucial importance. Despite their large theoretical storage capacity, utilizing these materials in rechargeable batteries in practice is not realized because of factors such as rate limitation and low electronic conductivity. It has been proposed that achieving controlled particle size and controlled morphology will improve the electrochemical performance of LiMPO₄ materials.[6,36] Therefore, improved understanding of the structure on the reduced dimensionality is highly desired not only for integrating these materials into technological applications but also for the fundamental reason that the growth, crystal structure, surface morphology, and chemical composition of the materials significantly affect their electrochemical performance. In this context, we have made attempts to understand the physical, geometric, and chemical structure of as-grown lithium nickel phosphates using the high-resolution transmission electron microscopy (HRTEM), selected area electron diffraction (SAED), energy-dispersive X-ray (EDX) spectrometry, and elemental compositional mapping using high-angle angular dark field scanning transmission electron microscopy (HAADF-STEM) and local structure and chemical bonding using Raman spectroscopy. The techniques based on the electron microscopy, imaging, and chemical analysis are well-suited to study the microstructure, phase purity, and chemical quality of materials on the micro- to nanosize and atomic level.[37–39] While HRTEM provides information on the lattice resolution structural quality of the sample, SAED is useful to probe

(16) Saidi, M. Y.; Huang, H.; Swoyer, J. L.; Barker, J. Lithium metal phosphates-next generation materials. Presented at 20th International Seminar and Exhibit on Primary and Secondary Batteries, Fort Lauderdale, FL, March 2002.
(17) Morgan, D.; Van der Ven, A.; Ceder, G. *Electrochem. Solid-State Lett.* **2004**, *7*, A30.
(18) Deniard, P.; Dulac, A. M.; Rocquefelte, X.; Grigorova, V.; Lebacq, O.; Pasturel, A.; Jobic, S. *J. Phys. Chem. Solids* **2004**, *65*, 229.
(19) Zhou, F.; Marianetti, C. A.; Cococcioni, M.; Morgan, D.; Ceder, G. *Phys. Rev. B* **2004**, *69*, 201101.
(20) Zhou, F.; Cococcioni, M.; Kang, K.; Ceder, G. *Electrochem. Commn.* **2004**, *6*, 1144.
(21) Xu, Y.-N.; Ching, W. Y.; Chiang, Y.-M. *J. Appl. Phys.* **2004**, *95*, 6583.
(22) Tang, P.; Holzwarth, N. A. W. *Phys. Rev. B* **2003**, *68*, 165107.
(23) Chupis, I. E. *Low Temp. Phys.* **2000**, *26*, 419.
(24) Kornev, I.; Bichurin, M.; Rivera, J.-P.; Gentil, S.; Schmid, H.; Jansen, A. G. M.; Wyder, P. *Phys. Rev. B* **2000**, *62*, 12247.
(25) Karchenko, N. F.; Karchenko, Yu. N.; Szymczak, R.; Baran, M.; Schmid, H. *Low Temp. Phys.* **2001**, *27*, 895.
(26) Karchenko, N. F.; Desnenko, V. A.; Karchenko, Yu. N.; Szymczak, R.; Baran, M. *Low Temp. Phys.* **2002**, *28*, 646.
(27) Karchenko, Y. N.; Karchenko, N. F.; Baran, M.; Szymczak, R. *Low Temp. Phys.* **2003**, *29*, 579.
(28) Kornev, I.; Rivera, J.-P.; Gentil, S.; Jansen, A. G. M.; Bichurin, M.; Schmid, H.; Wyder, P. *Physica B* **1999**, *271*, 304.
(29) Kornev, I.; Bichurin, M.; Rivera, J.-P.; Gentil, S.; Schmid, H.; Jansen, A. G. M.; Wyder, P. *Phys. Rev. B* **2000**, *62*, 12247.
(30) Vankin, D.; Zaretsky, J. L.; Miller, L. L.; Rivera, J.-P.; Schmid, H. *Phys. Rev. B* **2002**, *65*, 224414.
(31) Goni, A.; Lezama, L.; Barberis, G. E.; Pizarro, J. L.; Arriortua, M. I.; Rojo, T. *J. Magn. Magn. Mater.* **1996**, *164*, 251.
(32) Wilcke, S. L.; Cairns, E. J.; Reimer, J. A. *Solid State Nucl. Magn. Reson.* **2006**, *29*, 199.
(33) Paraguassu, W.; Freire, P. T. C.; Lemos, V.; Lala, S. M.; Montoro, L. A.; Rosolen, J. M. *J. Raman Specrosc.* **2005**, *36*, 213.
(34) Butt, G.; Sammes, N.; Tompsett, G.; Yamamoto, Y. *J. Power Sources* **2004**, *132*, 74.
(35) Garcia-Moreno, O.; Alvarez-Vega, M.; Garcia-Alvardo, F.; Garcia-Jaca, J.; Gallardo-Amores, J. M.; Sanjuan, M. L.; Amador, U. *Chem. Mater.* **2001**, *13*, 1570.

(36) Huang, H.; Yin, S.-C.; Nazar, L. F. *Electrochem. Solid-State Lett.* **2001**, *4*, A170.
(37) Utsunomiya, S.; Ewing, R. C. *Environ. Sci. Technol.* **2003**, *37*, 786.
(38) Ramana, C. V.; Utsunomiya, S.; Ewing, R. C.; Julien, C. M.; Becker, U. *Phys. Status Solidi A* **2005**, *202*, R108.
(39) Utsunomiya, S.; Palenik, C. S.; Ewing, R. C. In *Encyclopedia of Nanoscience and Nanotechnology*; Schwartz, J. A., Contescu, C. S., Putyera, K., Eds., Marcel Dekker, Inc.: New York, 2004; p 1087.

the crystal structure. Energy-dispersive X-ray spectroscopy (EDS) provides the information on the elements and impurities present in the sample. HAADF-STEM imaging is also a powerful method for chemical quality analysis as the chemical imaging is based on locating and studying the particles of interest in the selected dimensions, and image contrast is strongly correlated with the atomic number.[39] On the other hand, Raman spectroscopy is highly useful to probe the local structure, chemical bonding, and vibrational properties of the materials. The information obtained using these methods will be useful to better optimize the synthesis procedure of complex frameworks. Using the results obtained on $LiNiPO_4$, we discuss the structural quality and chemical homogeneity of the olivine specimens in relevance to their application in battery technology.

II. Experimental Section

A. Synthesis. *LiNiPO_4 Olivine.* The $LiNiPO_4$ phospho-olivine was prepared as microcrystalline powder by a conventional solid-state chemical reaction (SSCR) between Li_2CO_3, $(NH_4)_2HPO_4$, and NiO (Fluka, purum grade) raw materials. Stoichiometric amounts of reactants were mixed and carefully grinded. The mixture was pre-sintered at 120 °C for 12 h and then heated at 500 °C for 4 h. This thermal treatment causes the departure of exhausted gas according to the relation

$$2NiO + 2(NH_4)_2HPO_4 + Li_2CO_3 \rightarrow 2LiNiPO_4 + 4NH_3\uparrow + CO_2\uparrow + 2H_2O\uparrow \quad (1)$$
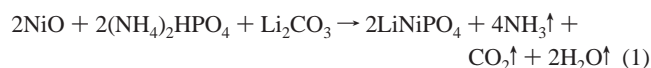
The decomposed powders were ground again and calcined in air at 800 °C for 48 h. The final product was cooled slowly to room temperature (RT).

Delithiated Li_0.09NiPO_4. The $Li_{0.09}NiPO_4$ olivine phase was prepared by chemical delithiation using the Wizansky et al.'s method.[40] The chemical delithiation experiments were conducted at a temperature of 55 °C, which is above RT. Oxidation of Ni was made using 1 equiv of nitronium hexafluorophosphate salt NO_2-PF_6 in acetonitrile under an argon atmosphere. The NO_2^+/NO_2 couple appeared at 5.1 V versus Li^0/Li^+. The mixture was stirred at RT for 24 h. The powders were washed and dried at 80 °C. The $x(Li)$ content was verified by inductively coupled plasma and X-ray diffraction (XRD) measurements. Both methods gave the same value of $x = 0.09 \pm 0.01$.

B. Characterization. *Transmission Electron Microscopy (TEM) Measurements.* TEM analysis was performed using a JEOL TEM2010F at a 200 kV acceleration voltage. Phase and structure of the material were monitored using SAED. The composition was analyzed by EDS in the TEM column utilizing EDAX Genesis software. The specimen for TEM analysis was prepared by dispersing the sample on a 3-mm Cu grid with a hole size of 1 × 2 mm. HRTEM and elemental mapping were completed by HAADF−STEM using Emispec ES Vision, version 4.0, of the STEM−EDX mapping system. To minimize the effect of sample drift, a drift-correcting mode was used during the acquisition of EDX maps. Specifications of STEM are listed as follows: Cs is 1.0 mm, the probe size is 0.5 nm for analysis and 0.2 for high-resolution imaging, the collection angle of the HAADF detector is 50−110 mrad, the objective aperture size is 30 μm for analysis and 20 μm for high-resolution imaging, the defocus condition is

(40) Wizansky, A. R.; Rauch, P. E.; DiSalvo, F. J. *J. Solid State Chem.* **1989**, *81*, 203.
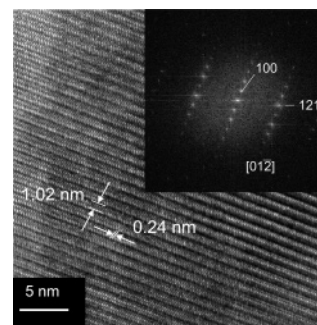
Figure 2. HRTEM image of $LiNiPO_4$. The well-resolved lattice fringes indicate the crystallinity of the sample. The measured values of the lattice fringe spacing are indicated. Inset shows the FFT of the HRTEM image, which indicates the direction in which the crystallite was examined and lattice planes contributing to the diffraction.

approximately −55 nm. Image processing including the fast Fourier transformation (FFT) was carried out by Gatan Digital Micrograph 3.4.

XRD and Raman Spectroscopy Measurements. XRD patterns of chemically synthesized $LiNiPO_4$ olivine and delithiated $Li_{0.09}NiPO_4$ samples were obtained using a Philips X′Pert PRO MRD (PW3050) diffractometer equipped with a Cu anticathode (Cu Kα radiation λ = 1.540 56 Å) at RT. The measurements have been recorded under Bragg−Brentano geometry at 2θ with a step of 0.05° in the range of 10−50°. Raman spectra were recorded on a Jobin-Yvon U1000 double monochromator using the 514.5 nm line from a Spectra-Physics 2020 argon-ion laser. Standard photon-counting techniques were used for detection. In a typical spectral acquisition, six Raman scattering (RS) spectra, each recorded with a resolution of 2 cm^{-1}, were averaged. Care was taken against sample photodecomposition using a low excitation power of 10 mW.

III. Results and Discussion

A. Electron Microscopy and Chemical Imaging. *TEM and HRTEM.* The TEM results of $LiNiPO_4$ indicated the presence of well-defined particles. The bright field TEM images indicate that the material contains microcrystallites. The corresponding scanning electron microscopy images (not shown) exhibit crystallites on the order of a few hundred nanometers in size. This result is consistent with observations of XRD where the patterns indicated the formation of well-crystallized particles with the estimated average size of 0.25 μm from the Scherrer's formula.

The HRTEM micrograph of $LiNiPO_4$ is shown in Figure 2. The inset shows the FFT of the selected region of the HRTEM image. The lattice fringes observed in the HRTEM image indicate that the synthesized $LiNiPO_4$ is well-crystallized. The lattice fringe spacing is 1.02 nm along the vertical direction. This value is comparable to the unit cell parameter along the crystallographic *a* direction, a = 1.03 nm of $LiNiPO_4$.[16] Therefore, the observed lattice spacing in the HRTEM image is attributed to the *a* lattice constant of $LiNiPO_4$. Similarly, the measured value of the lattice fringe spacing in the horizontal direction is 0.24 nm, which corresponds to the reflection from the (121) lattice planes of $LiNiPO_4$. The measured values of the lattice fringe spacing are indicated in Figure 2. The FFT (inset) indicates that the particle is being viewed along the (012) direction. It is important to recognize that the lattice resolution using HRTEM of $LiNiPO_4$ does not reveal any lattice defects such as dislocations and misfits. The lattice fringes are uniform
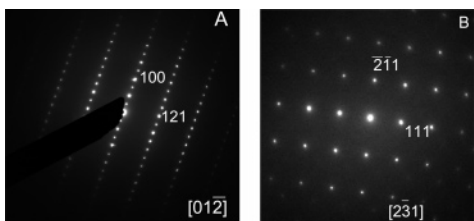
Figure 3. SAED patterns of LiNiPO₄. The assignment of diffraction maxima and the direction of view are indicated.

and continuous without any terminating lines or misalignment or any surface modulations. This is an indication of the structural quality of the material as the high density of such lattice defects or nonuniform microstructure will usually be observed in the HRTEM if they are incorporated as part of either during synthesis or handling of the sample. However, this characteristic feature of our sample cannot be compared to those reported earlier in the literature as HRTEM data is absent in other studies. Perhaps, the absence of secondary component phases even at a minor level could be the result of formation of such a defect free material.

SAED. The SAED patterns of LiNiPO₄ are shown in Figure 3. Figure 3A is the corresponding SAED pattern of LiNiPO₄ obtained in the same position of HRTEM measurements shown in Figure 2. The SAED patterns indicate the diffraction maxima, which are indexed according to crystallographic data of LiNiPO₄.[41] The diffraction maxima are identified as due to reflections from the lattice planes of (100) and (121) of the LiNiPO₄ olivine structure in the orthorhombic system as marked in Figure 3A. The diffraction pattern is a representation of the reciprocal lattice. Therefore, the large distance between the diffraction maxima in the horizontal direction indicates the relatively smaller value of interplanar distance. Similarly the small separation in the vertical direction is representative of the large interplanar distance of the lattice planes. In the present case, the diffraction maxima were identified as the reflections of the (100) and (121) lattice planes with a measured separation of 1.02 nm (long) and 0.24 nm (short) between the diffraction maxima, in vertical and horizontal directions, which are in good agreement with those reported (1.03 and 0.24 nm, respectively)

for LiNiPO₄.[41] The SEAD pattern shown in Figure 3B is obtained by aligning the incident electron beam to a different direction. The diffraction maxima observed are indicated in the image and match well with the structure reported for olivine LiNiPO₄ in the literature.[41]

Chemical Analysis and Elemental Mapping. The compositional analysis carried out by EDS measurements indicate that the LiNiPO₄ materials calcined at 850 °C for 48 h are highly stoichiometric with a chemical composition well-maintained upon heat treatment. The chemical composition analysis provides evidence for the formation of the stoichiometric LiNiPO₄ phase with uniformity and homogeneity of the sample maintained perfectly all over the sample prepared by SSCR. Similar results have been obtained by elemental mapping. The EDS spectrum of LiNiPO₄ is shown in Figure 4. The spectrum (left panel) exhibits the characteristic peaks of Ni, P, and O present in the sample. It is not possible to detect Li for the obvious reason that the X-ray fluorescence yield is extremely low for the elements Li and Be.

The EDS measurements can be used to qualitatively discuss the structural and chemical quality of the SSCR LiNiPO₄. To obtain the qualitative information on the chemical composition of the grown oxide, we have carefully positioned the sample in the TEM column and recorded the EDS spectra of the sample to avoid any additional contamination. The respective peaks due to Ni, P, and O are indicated in the spectrum along with their respective energy positions. It is well-known that the X-ray energy is characteristic of generating atoms in the sample.[39] Therefore, the detection of X-rays emitted from the sample as a result of sample−electron beam interaction provides the identification of the atoms present in the lattice. The lines identified are O $K\alpha_1$, P K_α, Ni K_α, Ni K_β, Ni L_α, and Ni L_β, respectively. The contributions from the Cu grid can also be seen in the spectrum (Figure 4). It is hard to eliminate the contribution from the supporting Cu grid, but it can be used as a reference. It is evident from the EDS spectrum that the characteristic X-ray peaks due to Ni, P, and O are the only contributions. The presence of peaks due to other elements either as dopants or as impurities is not detected, which is an indication of the
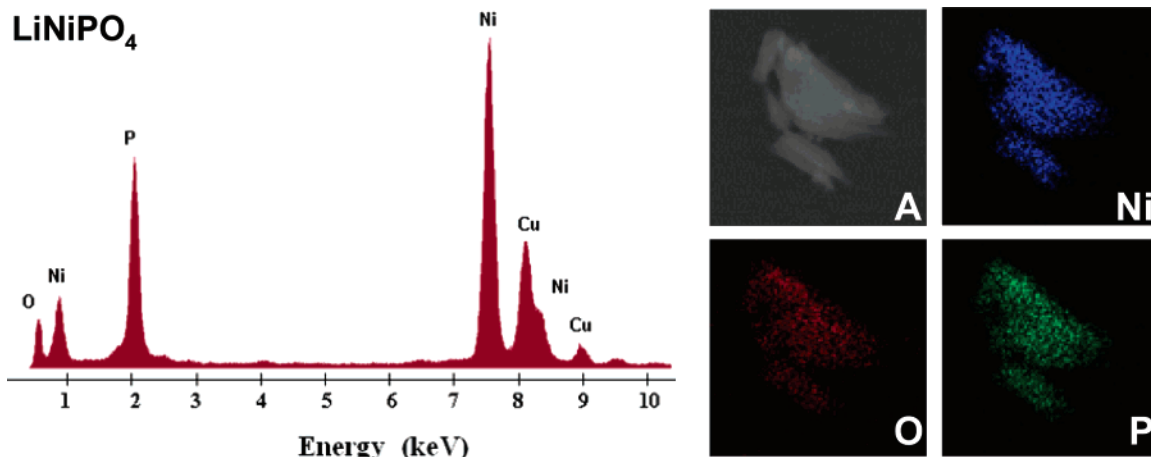
Figure 4. EDS spectra and compositional mapping images of LiNiPO₄. The left panel shows the EDS spectrum of LiNiPO₄. The peaks due to O, Ni, and P in the sample are indicated. The peaks due to the supporting Cu grid can also be seen (see the text for description). The right panel shows the elemental mapping images of the sample obtained using HAADF-STEM. The HAADF-STEM image of the particle (A) and mapping of the elements Ni, O, and P are indicated.
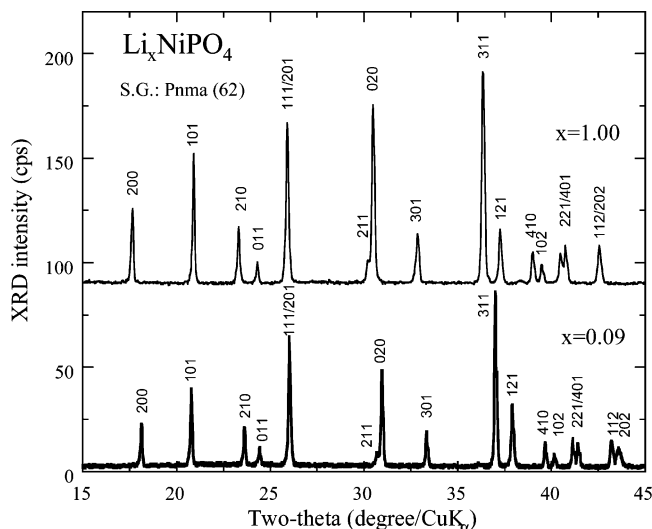
Figure 5. XRD diffractograms for the $LiNiPO_4$ olivine sample and delithiated $Li_{0.09}NiPO_4$ sample. Lines are indexed in the orthorhombic system (*Pnma* space group, No. 62).

Table 1. Factor Group Analysis for the Olivine $LiNiPO_4$, *Pnma* Space Group (D_{2h})[16] in which (R), (IR), and (in) Represent Raman and Infrared-active Vibrations and Inactive Modes, Respectively

		Translations of Li, Ni, and P Atoms
atom	site group	factor group D_{2h}
Li (4a)	C_i	$3A_u + 3B_{1u} + 3B_{2u} + 3B_{3u}$
Ni (4c)	C_s^{xz}	$2A_g + B_{1g} + 2B_{2g} + B_{3g} + A_u + 2B_{1u} + B_{2u} + 2B_{3u}$
P (4c)	C_s^{xz}	$2A_g + B_{1g} + 2B_{2g} + B_{3g} + A_u + 2B_{1u} + B_{2u} + 2B_{3u}$

		Internal Modes of PO_4
point group T_d	site group C_s^{xz}	factor group D_{2h}
A_1	A'	$A_g + B_{2g} + B_{1u} + B_{3u}$
E	$A' + A''$	$A_g + B_{1g} + B_{2g} + B_{3g} + A_u + B_{1u} + B_{2u} + B_{3u}$
F_2	$2A' + A''$	$2A_g + B_{1g} + 2B_{2g} + B_{3g} + A_u + 2B_{1u} + B_{2u} + 2B_{3u}$
F_2	$2A' + A''$	$2A_g + B_{1g} + 2B_{2g} + B_{3g} + A_u + 2B_{1u} + B_{2u} + 2B_{3u}$

		Librations of PO_4
point group T_d	site group C_s^{xz}	factor group D_{2h}
F_1	$A' + 2A''$	$A_g + 2B_{1g} + B_{2g} + 2B_{3g} + 2A_u + B_{1u} + 2B_{2u} + B_{3u}$

Total Amount of Allowed Optical Modes ($N = 3n - 3 = 81$)
$\Gamma = 11A_g(R) + 7B_{1g}(R) + 11B_{2g}(R) + 7B_{3g} +$
$10A_u(in) + 13B_{1u}(ir) + 9B_{2u}(ir) + 13B_{3u}(ir)$

sample chemical purity. These results suggest that the chemical reaction process induced impurities are absent in the grown sample.

The elemental mapping images of $LiNiPO_4$ obtained using HAADF-STEM imaging are shown in the right panel of Figure 4. The image of the representative particle used to obtain the elemental analysis is also shown (image A). The images labeled Ni, P, and O represent the elemental mapping of the respective elements. These images are uniform along the shape of the particle examined. They show that characteristic X-rays emit from Ni, P, and O simultaneously from the same location of point and region, which is an indicative of the chemical homogeneity of the SSCR-grown $LiNiPO_4$ sample. The distribution is further characterized by the uniform elemental composition distribution throughout the sample. Such a uniform chemical distribution and homogeneity is important to employ the materials for battery application.

B. XRD. The XRD patterns of the Li_xNiPO_4 ($x = 1.00$ and 0.09) samples are reported in Figure 5. The Miller indexes (*hkl*) of the diffraction peaks, determined from their position given by ASTM, are also indicated. It is evident from the XRD pattern (Figure 5) that the pristine $LiNiPO_4$ material prepared by solid-state reaction at 850 °C exhibits a single phase with an olivine-like structure. The TEM, SAED, and XRD studies confirm the formation of a stable olivine structured $LiNiPO_4$ phase. The notable feature of the XRD patterns for the pristine and delithiated samples is a relative shift in the peak positions. The shift in the position of the XRD peaks for Li_xNiPO_4 ($x = 0.09$) when compared to that of the pristine material ($LiNiPO_4$; $x = 1$) is due to the contraction of the lattice upon delithiation, as evidenced by the unit-cell parameters.

The quantitative measurements of the lattice parameters using XRD provided interesting information on the structure of both the pristine and the delithiated samples. For $x = 1$,

(41) Abrahams, I.; Easson, K. S. *Acta Crystallogr., Sect. C* **1993**, *49*, 925. Data 81-1528 reported by American Society for Testing Materials file for $LiNiPO_4$.

the refinement of the XRD data gives the unit-cell parameters (in the *Pnma* orthorhombic space group) $a = 1.037(1)$ nm, $b = 0.5867(8)$ nm, and $c = 0.4680(1)$ nm. The numbers in the parentheses indicate the accuracy. These values for $LiNiPO_4$ are found in quantitative agreement with those previously reported by Abrahams and Easson[41] and Santoro et al.[3] It should be noted that no peak of an extrinsic nature has been detected on the SSCR $LiNiPO_4$ sample, which indicates that the amount of NiO and Li_3PO_4, if any, is so small that it is not at all detected. For $x = 0.09$ (delithiated sample), the unit-cell parameters are $a = 0.9973(7)$ nm, $b = 0.5579(9)$ nm, and $c = 0.4785(6)$ nm. In addition to the contraction of the lattice we also noticed a distortion because c is found actually larger in the delithiated ($x = 0.09$) sample. This can be viewed as a change in the Jahn−Teller distortion of the lattice associated with a change in the chemical valence state of Ni, which is Ni^{2+} with an orbital moment $L = 3$ in the $x = 1$ case and Ni^{3+} ($L = 3$) in the $x = 0.09$ sample.

It is important to compare and contrast our results with the available reports in the literature, particularly with those predicted by the computations for $LiMPO_4$ (M = Fe, Co), to understand the Li deinsertion reaction process and contraction of the lattice upon delithiation. In the present work, the change in the unit cell volume after Li removal with nitronium salt reveals a contraction as expected by the computed work of Ceder et al.[20] Our experimental results can be compared with calculated unit-cell volume changes (see Table 1 in ref 20). The cell volume contraction from 285 to 266 $Å^3$ ($\Delta V \approx 6\%$) is significantly larger than that calculated from the best GGA+U results (from 282 to 279 $Å^3$)[20] but slightly smaller than those calculated from the standard LDA or GGA methods (from 283 to 260 $Å^3$). However, it should be noted that the volume change $\Delta V = 5$ $Å^3$/formula unit is similar to that calculated for $LiCoPO_4$.

The chemical extraction of Li from the $LiNiPO_4$ olivine framework appears very effective with nitronium salt as the
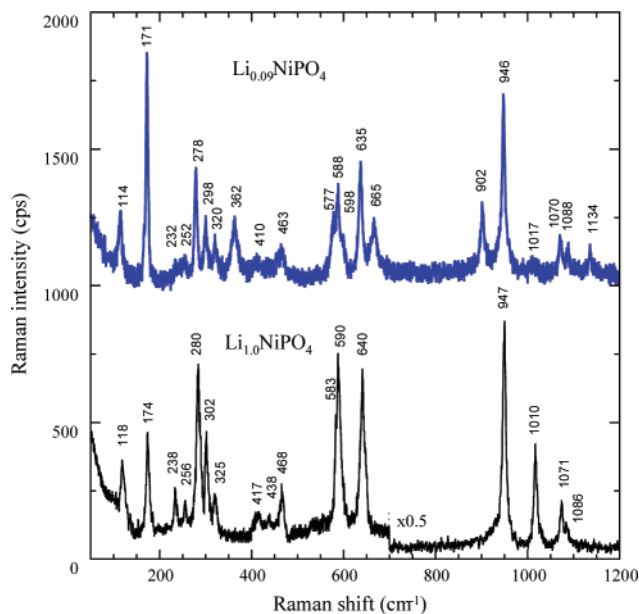
Figure 6. RS spectra of Li$_{1.0}$NiPO$_4$ and Li$_{0.09}$NiPO$_4$ samples.

NO$_2^+$/NO$_2$ couple which has a potential of 5.1.[40] Lithium extraction occurs at different potentials in LiMPO$_4$ olivine depending of the M^{2+}/M^{3+} redox couple. The potential has been experimentally determined at 3.45 V versus Li for LiFePO$_4$,[1] while LiCoPO$_4$ works below 5 V versus Li.[42] The voltage calculated by Ceder et al. with the GGA+U method was 5.07 V versus Li. It seems that kinetic factors play an important role in this reaction. Because LiNiPO$_4$ was deintercalated above RT, the chemical diffusion of Li$^+$ ions could be enhanced at 55 °C. In addition, the two-phase or phase mixture formation during the delithiation reaction is not ruled out in the present case as reported for other members of the family, LiMPO$_4$. Preliminary results on intermediate products (not shown here) show the co-existence of XRD patterns belonging to two-phase system that could indicate a two-phase reaction, that is, presence of the mixture LiNiPO$_4$ + NiPO$_4$, upon Li removal. This behavior has been early reported for LiFePO$_4$ by Padhi et al.[1] and more recently for LiCoPO$_4$ by Amine et al.[43] and Bramnik et al.[44]

C. Raman Spectroscopy. The local structure and chemical bonding in LiNiPO$_4$ and Li$_{0.09}$NiPO$_4$ materials have been investigated by Raman spectroscopic measurements. The RS spectra of Li$_x$NiPO$_4$ olivine phases for $x = 1$ and $x = 0.09$ are shown in Figure 6. The RS active bands are relatively narrow and well-resolved. The RS features can clearly be divided into two regions, above and below 400 cm^{-1}, that correspond to the domain of appearance of internal and external modes, respectively.[33−35,44−49] This description is acceptable for the olivine structure and makes it easy to

visualize the eigenmodes of different Raman and infrared (IR)-active modes. As the structure of phospho-olivine is built from LiO$_6$ and NiO$_6$ octahedral units linked to (PO$_4$)$^{3−}$ oxo-anions, the local cationic arrangement can be discussed with the aid of factor group analysis and the molecular vibration model.[44,45] The corresponding site symmetries in the Bravais cell for the D_{2h}^{16} (No. 62) spectroscopic symmetry that contain both IR and Raman active modes are given by

$$D_{2h}:^{16} 2C_i\,(4);\ C_s\,(4);\ C_1\,(8) \qquad (2)$$

Table 1 summarizes the group theoretical analysis carried out for the olivine-like structure. The olivine belongs to the spectroscopic symmetry D_{2h};[16] the primitive cell is centrosymmetric with four formula units in the cell. Li, Ni, and P atoms are distributed on the 4a, 4c, and 4c sites (Wyckoff notation), respectively. Subtracting the three acoustic modes ($B_{1u} + B_{2u} + B_{3u}$) from the total number of vibrations ($N_{tot} = 3n − 3 = 81$), the allowed optical modes are represented by

$$\Gamma_{(LiNiPO_4)} = \Gamma = 11A_g + 7B_{1g} + 11B_{2g} + 7B_{3g} + 13B_{1u} + \\ 9B_{2u} + 13B_{3u} \quad (3)$$

Out of the allowed modes, the even (gerade; g) and odd (ungerade; u) species are Raman and infrared-active modes, respectively. This treatment has been carried out by assuming the separation of the vibrations into internal (PO$_4$)$^{3−}$ and external (lattice) modes. The validity of this approximation has been examined in the past[46,47] and confirmed most recently by the experimental and theoretical approaches.[33−35,50] Paques-Ledent and Tarte conducted a comprehensive vibrational analysis of numerous olivine materials.[46] Fomin et al. have reported the Raman spectroscopic data of single-crystal LiNiPO$_4$ over a wide temperature range and have examined the validity of internal−external modes approximation in successfully analyzing the vibrational properties.[50] Paraguassu et al. have performed the phonon calculation of olivine-like LiMPO$_4$ (M = Ni, Co, Fe) using computational approach and have used the same approximation in reporting the Raman data for all the compounds.[33] Therefore, we discuss the present RS data of olivine LiNiPO$_4$ using the same approach. The internal modes involve the displacement of oxygen atoms of the tetrahedral (PO$_4$)$^{3−}$ anions and present frequencies closely related to those of the free molecule. For the free oxo-anion (PO$_4$)$^{3−}$, these are a singlet (A$_1$) at a frequency $\nu_1 = 938$ cm^{-1}; a doublet (E) at $\nu_2 = 465$ cm^{-1} and two triply degenerate (F$_2$) modes, ν_3 at 1027 cm^{-1}, and ν_4 at 567 cm^{-1}. ν_1 and ν_3 involve the symmetric and asymmetric stretching modes of the P−O bonds, whereas ν_2 and ν_4 involve mainly O−P−O symmetric and asymmetric bending modes with a small contribution of P vibration. For the LiNiPO$_4$ ($x = 1$) compound, the corresponding Raman bands located at 947, 468, 1071, and 590 cm^{-1}, respectively, are split in many components as a result of the correlation

(42) Wolfenstine, J.; Poese, B.; Allen, J. *J. Power Sources* **2004**, *138*, 281.
(43) Amine, K.; Yasuda, H.; Yamaki, M. *Electrochem. Solid-State Lett.* **2000**, *3*, 178.
(44) Bramnik, N. N.; Bramnik, K. G.; Buhrmester, T.; Baehtz, C.; Ehrenberg, H.; Fuess, H. *J. Solid State Electrochem.* **2004**, *8*, 558.
(45) Nakamoto, K. *Infrared and Raman spectra of inorganic and coordination compounds*; Wiley & Sons: New York, 1978.
(46) Paques-Ledent, M. T.; Tarte, P. *Spectrochim. Acta, Part A* **1973**, *30*, 673.
(47) Hezel, A.; Ross, S. D. *Spectrochim. Acta, Part A* **1967**, *23*, 1583.
(48) Walrafen, G. E.; Irish, D. E.; Young, T. F. *J. Chem. Phys.* **1962**, *37*, 662.

(49) Ait Salah, A.; Jozwiak, P.; Garbarczyk, J.; Benkhouja, K.; Zaghib, K.; Gendron, F.; Julien, C. M. *J. Power Sources* **2005**, *140*, 370.
(50) Fomin, V. I.; Gnezdilov, V. P.; Kurnosov, V. S.; Peschanski, A. V.; Yerementko, A. V.; Schmid, H.; Rivera, J.-P.; Gentil, S. *Low Temp. Phys.* **2002**, *28*, 203.

effect induced by the coupling of Ni$-$O units in the structure. The very sharp band at 946 cm^{-1} is attributed to ν_1, while the three weaker peaks are thought to belong to the asymmetric stretching modes of the $(PO_4)^{3-}$ anion (ν_3) In the region of the internal modes of the phosphate anion, we identify the symmetric stretching mode and triplets in the high-wavenumber region, while the far-infrared region (below 300 cm^{-1}) displays the external modes. The RS band around 640 cm^{-1} is assigned to the stretching mode of NiO_6 octahedra. As the frequency of this band appears to be proportional to the ionic radius of the divalent transition-metal cation, we can conclude that any component of the PO_4 groups contributes in this motion.[51]

The basic feature is that, upon delithiation, the frequencies of the vibrations show only a small shift (by a few inverse centimeters), which is the consequence of the change of the lattice parameters and also, below 700 cm^{-1}, the change in the nickel valence state. The extraction of lithium ions coordinated to the oxygen atoms of $(PO_4)^{3-}$ units causes a redistribution of electron density in the P$-$O bonds that produces modifications of the effective force constants and polarizability derivatives. If we try to follow up the shift of the mode frequencies, we can make a correspondence of the lines (in cm^{-1}), from $x = 1$ to $x = 0.09$: $417 \rightarrow 410$, $325 \rightarrow 320$, $280 \rightarrow 278$, $256 \rightarrow 252$, $238 \rightarrow 232$, $174 \rightarrow 171$, $118 \rightarrow 114$. This indicates that these modes are primarily translation and libration motions of the $(PO_4)^{3-}$ ions and translation motions of the Ni^{2+} ions. However, we do not observe any mode associated to the vibration of the lithium ions because in the crystal structure of $LiNiPO_4$, the lithium ions occupy $4a$ Wyckoff sites, which contain an inversion center. One interesting point is evidenced by the correlation effect. There is no Raman active species in the irreducible representation related to the Li atoms located on $4a$ sites (C_i symmetry) as sites with inversion symmetry are not Raman active. In other words, the Li atoms are not spectroscopically active and are not allowed to move during Raman active vibrations. This is in relation with the fact that these atoms are located on inversion centers of the crystal cell.[52] Recently, Garcia-Moreno et al. have also reported the fact that lithium is not Raman active in this phase based on the observation that the substitution of ^7Li by ^6Li in the olivine phase of $LiNiPO_4$ does not result in any remarkable change in the Raman spectrum.[35] Thus, any mode that involves lithium motion must be Raman inactive and IR active. However, on another hand, we observe the growth of an extra line at 364 cm^{-1}, while bands in the region 250$-$350 cm^{-1} decrease in intensity with the decrease of lithium content. In the intermediate range 400$-$600 cm^{-1}, we can assume that the modes at 577, 588, 598, 635, and 665 cm^{-1} correspond to the bending modes ($\nu_2 + \nu_4$) of the $(PO_4)^{3-}$ oxo-anions in $NiPO_4$. The $(PO_4)^{3-}$ symmetric stretching band in $LiNiPO_4$ at 947 cm^{-1} appears at 946 cm^{-1} in $Li_{0.09}NiPO_4$, while the asymmetric stretching ν_3 modes at 1010 cm^{-1} becomes very weak upon Li removal. The most notable feature of the RS spectrum of $Li_{0.09}NiPO_4$ is the appearance of new peaks in the high-wavenumber region at 902 and 1134 cm^{-1}. Two Raman-active modes ($A_g + B_{2g}$) are predicted by factor group analysis of $NiPO_4$ (*Pnma* space group). The band at 902 cm^{-1} is assigned to the symmetric B_{2g} mode of ν_1. These extra lines have been also observed in the RS spectra of Li_xFePO_4.[53] On the other hand, we can make the hypothesis that the mode at 1134 cm^{-1} is linked to a vibration mode of PO_3. The same vibration mode has also been observed in $R(PO_3)_3$ metaphosphates (R = Ga, In, Y, Sm, Gd, Dy) in the range 1230$-$1280 cm^{-1}.[54] The present data of olivine $LiNiPO_4$ are in good agreement with the earlier reports.[33$-$35,50] There were no reports on the delithiated $Li_{0.09}NiPO_4$ phase, and, therefore, such a comparison is not made.

IV. Summary and Conclusions

Lithium nickel phosphate materials were prepared by SSCR at 850 °C. The structural and chemical quality of as-grown $LiNiPO_4$ is studied using the analytical electron microscopy measurements. XRD and Raman spectroscopic measurements were used to support the discussion of the structural characteristics. The presence of well-defined lattice fringes in the HRTEM indicates that the sample is well-crystallized. The crystal structure of $LiNiPO_4$ is free from defects such as dislocations and misfits as indicated by the uniform lattice fringes without any discontinuity or terminations. The measured fringe spacing and indexing the corresponding electron diffraction pattern indicate that the structure of $LiNiPO_4$ is similar to the reported olivine structure in the literature. The EDX spectrometry and the elemental compositional mapping using HAADF-STEM revealed the high chemical quality of the grown $LiNiPO_4$ in terms of homogeneity and uniform distribution characteristics. The incorporation of impurities or dopants either due to processing or postprocess handling is not at all detected. XRD analysis confirms that the grown $LiNiPO_4$ material is microcrystalline with a particle size of about 0.25 μm and adopts the olivine structure. Raman spectroscopic measurements provided information on the bonding between NiO_6 octahedral and $(PO_4)^{3-}$ tetrahedral groups in $LiNiPO_4$. Analytical electron microscopy and chemical imaging analysis, along with XRD and Raman measurements, of the structure and chemical characteristics indicates that the grown $LiNiPO_4$ could be useful in the development of high energy density rechargeable batteries. Analysis of the delithiated $Li_{0.09}NiPO_4$ phase performed using XRD and Raman spectroscopic measurements indicates a contraction and distortion of the lattice upon lithium extraction.

CM061137C

(51) Ait Salah, A.; Zaghib, K.; Gendron, F.; Massot, M.; Julien, C. M. *Extented Abstracts of the 207th Electrochemical Society Meeting*, Québec, Canada, May 2005; Abstract 1349.
(52) Julien, C. *Ionics* **2000**, *6*, 30.
(53) Burba, C. M.; Frech, R. *J. Electrochem. Soc.* **2004**, *151*, A1032.
(54) Ilieva, D.; Koacheva, D.; Petkov, C.; Bogachev, G. *J. Raman Spectrosc.* **2001**, *32*, 893.